JAAS

Neptunium transition probabilities estimated through laser induced breakdown spectroscopy (LIBS) measurements

Journal:	*Journal of Analytical Atomic Spectrometry*
Manuscript ID	JA-ART-12-2021-000423.R1
Article Type:	Paper
Date Submitted by the Author:	11-Feb-2022

Complete List of Authors:	Andrews, Hunter; Oak Ridge National Laboratory, Radioisotope Science and Engineering Division Sadergaski, Luke; Oak Ridge National Laboratory, Radioisotope Science and Engineering Division Myhre, Kristian; Oak Ridge National Laboratory, Radioisotope Science and Engineering Division

Neptunium transition probabilities estimated through laser induced breakdown spectroscopy (LIBS) measurements

H. B. Andrews‡, L. R. Sadergaski, and K. G. Myhre

Oak Ridge National Laboratory, 1 Bethel Valley Rd., Oak Ridge, TN 37830, USA

‡Corresponding author: andrewshb@ornl.gov

Received date: 12, 06, 2021

Abstract

Calibration free–laser induced breakdown spectroscopy (CF-LIBS) approaches are promising for the analysis of radioactive materials; however, a lack of reported fundamental properties for these materials is an obstacle to implementation. Spectra of laser induced plasmas containing Np and Sr, along with Saha–Boltzmann methods, were used to estimate the first reported transition probabilities (TPs) of Np. These TPs enabled the first attempt at CF-LIBS analysis of radioactive samples to predict Np/Sr ratios with a mean error of 3.86%. The presented methodology of TP estimation will be applied to the study of other actinides and allow broader applications of CF-LIBS in the nuclear field.

Keywords: laser induced breakdown spectroscopy (LIBS), calibration free laser induced breakdown spectroscopy (CF-LIBS), transition probability, neptunium, strontium, Saha–Boltzmann, laser induced plasma, actinide

I. INTRODUCTION

Optical spectroscopy techniques frequently offer analytical benefits including being completely or nearly nondestructive, highly sensitive to multiple elemental or molecular signatures simultaneously, and being capable of rapid in-situ analysis in hazardous environments [1]. Laser induced breakdown spectroscopy (LIBS) is a form of optical spectroscopy performed by focusing

a nanosecond pulsed laser onto a sample surface. The laser energy rapidly heats the sample surface, resulting in the ablation of a few nanograms of material and subsequent formation of a plasma plume. Light characteristic of electronic transitions occurring in the plasma as it cools is emitted and can be analyzed with a spectrometer. The resulting spectrum is rich in elemental information as LIBS can be used to analyze for the presence and concentration of nearly all elements in the periodic table [1–3]. The robustness of LIBS makes it ideal for rapid analysis in field deployed applications as well as in hazardous environments because of its ability to be performed remotely using long-range optics or optical fibers [1,4].

Traditional LIBS relies on matrix matched calibration models that can be laborious and, in some cases, difficult to develop when there is a lack of available materials [3,5]. To overcome this weakness, calibration free–LIBS (CF-LIBS) procedures have been developed, which rely on fundamental physics–based plasma relationships to correlate relative concentration to peak intensities [5]. These methods can overcome matrix effects and provide rapid analysis without the need for a traditional calibration model. Although there is not a need for a calibration model, certain characteristics of any given electronic transition need to be defined, including upper energy level, upper-level degeneracy, and the transition probability (TP). The former two are generally available, but many heavy elements lack reported TPs because of the expensive experimental systems needed to perform the measurements or a lack of available analyte, which is also a difficulty for traditional LIBS. A common method to determine TPs is to use a constant light source, such as a hollow-cathode lamp which is a particular issue for actinide materials [6]. For actinides, most in the series have few-to-no reported TPs relevant to laser induced plasmas [7,8].

This is concerning because CF-LIBS would be a valuable tool for analysis in many process applications found in radioisotope production from used nuclear fuel. These applications would

benefit from rapid elemental analysis without the need for calibration. The ability to perform LIBS via fiber optics makes it ideal for monitoring hot cell processes. One example includes producing ^{238}Pu for NASA's radioisotope thermoelectric generators, which is used to provide power for deep space missions [9]. This production stream includes irradiating ^{237}Np targets at Oak Ridge National Laboratory's (ORNL) High Flux Isotope Reactor. The ^{237}Np absorbs a neutron and then goes through a beta decay to transmutate to ^{238}Pu. These targets are then processed in radiochemical hot cells at ORNL's Radiological Engineering Development Center to separate the ^{238}Pu from the ^{237}Np. The efficiency of this process is dependent on the purity of the ^{237}Np targets, so there is an opportunity for CF-LIBS to aid in impurity analysis throughout this process.

Therefore, the goal of this study was to measure the TPs of Np from spectra of laser induced plasmas and to demonstrate the capability to perform CF-LIBS with small quantities of actinide materials. Typically, CF-LIBS is performed with nanosecond exposure times; however, the equipment available for this study is only capable of microsecond level exposure times [10, 11]. Therefore, this study sets out to investigate if an effective version of CF-LIBS can be applied despite this discrepancy. Mixtures of Np and Sr were measured with typical LIBS methods. Here, Sr was chosen to serve as an internal reference analyte because of the large number of spectral lines with well-defined properties (e.g., TPs with high accuracies). The resultant spectra were analyzed using Saha–Boltzmann relationships to determine the first reported TPs of neutral and singly ionized Np.

II. EXPERIMENTAL

Three samples were prepared in a radiological hood by pipetting 0.10 M Np and 0.05 M Sr stock solutions onto the surface of an Al puck with a 0.16-in. divot in the center to help the droplet remain centered. A 10 μL droplet of a mixed stock solution was dried onto the surface of the puck

before another droplet was placed in the same location. This was repeated three times per sample to ensure an adequate amount of material was layered at the measuring point. The final three samples had Np/Sr molar ratios of 8.0, 2.0, and 1.0, respectively. Again, here Sr is used as an internal reference for calculating the Np TPs. It was selected due to the large number of available peaks with accurate TPs, but other elements could be used in future cases where Sr is an interferent. These samples were inserted into 3D-printed containers, which were sealed by threading a lid down onto a Thorlabs wedged window (WW42012-C) with an O-ring between the window and the container body. An illustration of the sample preparation procedure and radiological sample enclosure is shown in Fig. 1.

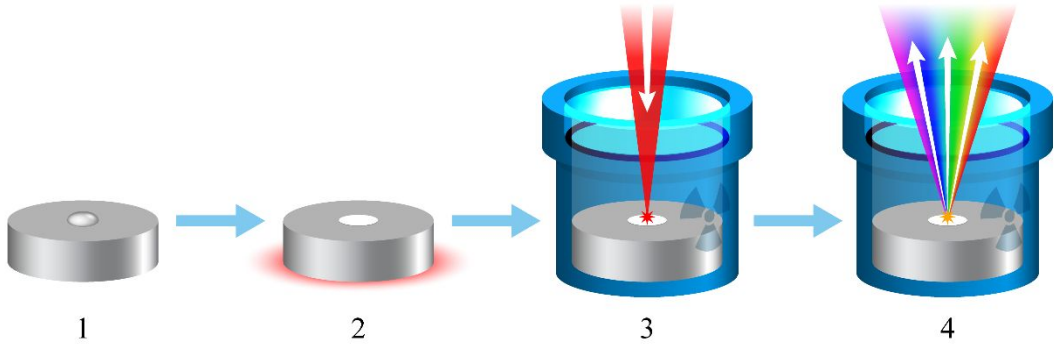

Fig. 1. Illustration of sample preparation involving the following steps: (1) a droplet is placed on the center spot of an aluminum puck; (2) the droplet is dried, depositing the analyte onto the surface; (3) the sample is inserted into a sealed radiological enclosure and excited using an incident pulsed laser; and (3) a microplasma is formed and subsequent atomic emissions are collected for measurement.

The sealed sample containers were then placed into the laser enclosure of an Applied Photonics LIBSCAN 150 laser system for analysis. This system uses a 1064 nm, 161 ± 2.25 mJ,

~5 ns pulsed Nd:YAG laser to perform laser ablation [12]. The sample enclosure contains mounted collimating optics at a small angle to the impending laser pulse. Through fiber optics, the collected light was routed to a Catalina Scientific Instruments EMU-120/65 echelle spectrometer equipped with a Raptor Falcon Blue EMCCD camera (λ/FWHM ≈ 12,000) for analysis. This setup relies on a Quantum Composers pulse generator to control the delay time between lasing and initiating light collection. Additionally, a Hg(Ar) lamp (SL2) and a certified W halogen lamp (SL1-CAL) from StellarNet were used for wavelength calibration and relative efficiency correction.

The samples were positioned at the laser focal point via a motorized XYZ translation stage, which allowed the analysis of nine locations to help account for variations in the deposited material. Each spot was shot five times before the deposited sample was consumed. The measurements were taken with a delay time of 0.1 μs and an integration time of 100 μs. All spectral analysis was completed using Python 3 [13].

III. RESULTS AND DISCUSSION

A. Spectral preprocessing

The first step in the analysis of the collected spectra was to account for wavelength variations in measurement efficiency. This relative efficiency curve was calculated by comparing the certified spectrum of the W halogen lamp to the spectrum measured by the echelle spectrometer with all optical components inline. This included the wedged window, the collimating optics, and the fiber optics. The resultant relative efficiency curve is shown in Fig. 2(a). Wavelengths <350 nm were not included in this analysis because of the lack of signal from the calibrated light source and the inability to calculate the spectrometer efficiency of this region.

Approximately 3 min elapsed for each sample measurement. Each set of five sequential spectra were averaged to provide one spectrum per shot location and nine spectra per sample. This helped account for small variations in laser energy and variations of material in each shot as the deposited material was consumed by ablation. Next, the spectra were background corrected using an algorithm, similar to the one offered by Yaroshchyk and Eberhardt [14]. The minimum spectral intensity of every 50 data points in the spectra (comprising 1 nm) were recorded in a list. A line was then fit to this list of points and smoothed using a Savitzky–Golay filter with a window of 11 nm and a polynomial order of five. The resultant baseline was then subtracted from the corresponding spectrum. The last preprocessing step was to normalize the spectra to the 383 nm Al I peak to adjust for any variations in shot-to-shot laser energy. An example spectrum for sample 1 (8.0 Np/Sr) after preprocessing is shown in Fig. 2(b)-(d).

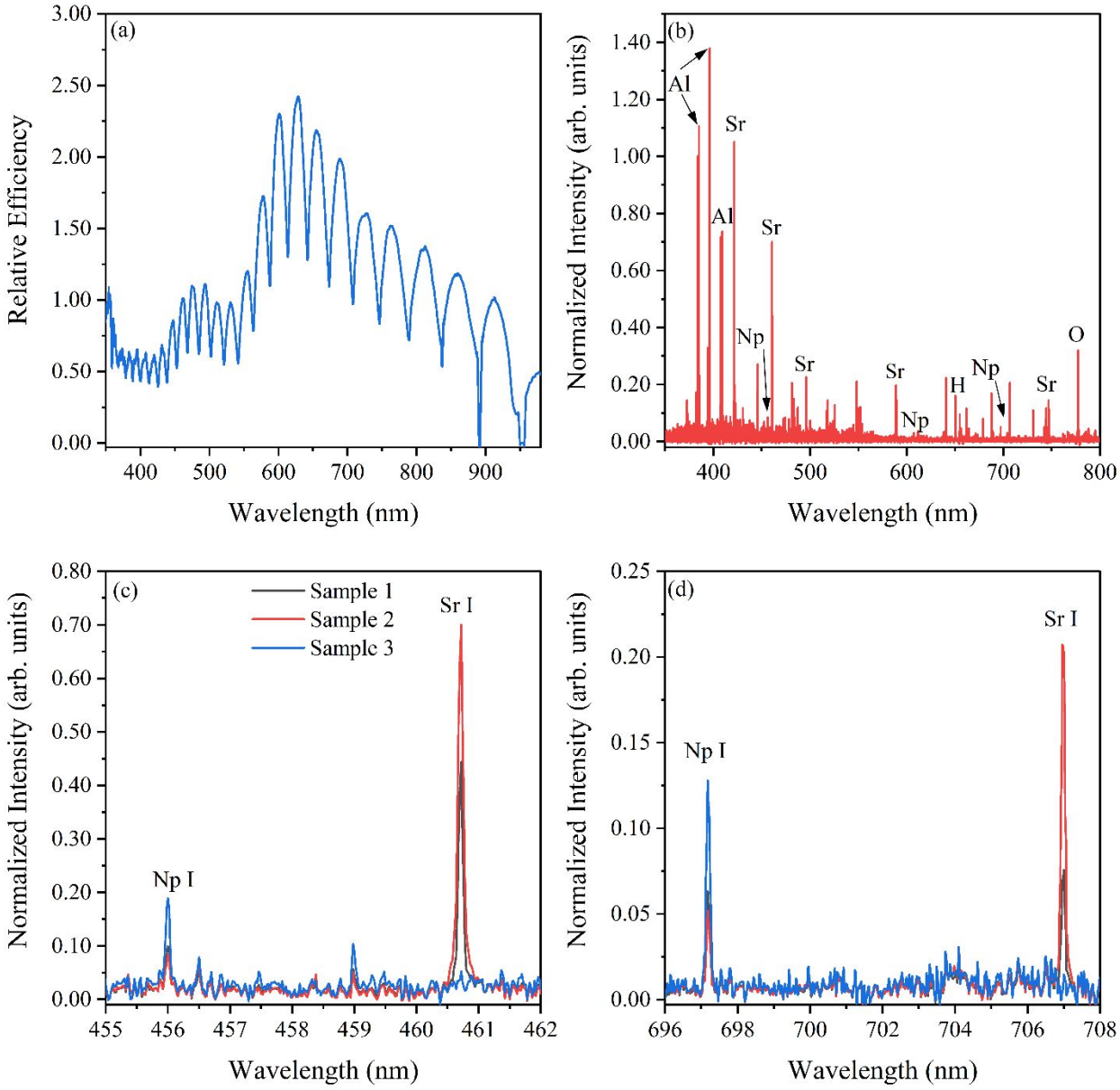

Fig. 2. (a) The calculated relative efficiency curve and (b) an example spectrum from sample 1 (8.0 Np/Sr) after preprocessing. Zoomed plots showing neutral Np and Sr peaks are shown in (c) and (d).

The processed spectra were investigated to identify Sr peaks with TPs reported in the National Institute for Standards and Technology (NIST) Atomic Spectra Database [7]. Several Sr peaks were found, but many suffered from apparent self-absorption and were discounted from the analysis. It is important to note that there are many studies on how to correct for self-absorption

effects; the reader is pointed to a paper by Borges et al. for further discussion [11]. A decision to not correct the lines suffering from self-absorption was made for two main reasons. First, the Stark coefficients for these Sr lines were not reported. Second, other correction methods such as using the ratio of intensities, degeneracies, and TPs force the Saha-Boltzmann line to a near perfect fit [11]. While this is very useful for CF-LIBS, in this study the Sr Saha-Boltzmann fit was used to estimate the Np TPs and these correction methods may have artificially reduced the uncertainty of these calculated values.

Information on the selected seven Sr peaks is presented in Table I. To identify Np peaks, first, all potential transition wavelengths were calculated by taking the difference between all neutral and singly ionized energy levels from the NIST Basic Atomic Spectroscopic Database [7]. Then spectra with varying Np/Sr ratios were scanned to find peaks that showed both an intensity correlation with this ratio and matched the calculated wavelengths, such as the peaks seen in Fig. 2(c) and 2(d). Information on the identified Np peaks is also shown in Table I. The identified Np peaks match emission lines reported by DeKalb and Edelson from a Np inductively coupled plasma [15]. The two Np peaks reported from the LIBS spectrum of a mixed actinide sample were not seen in this study's spectra; however, this may be due to their proximity to the lower efficiency wavelength region (~350 nm) [16].

Table I. List of identified Sr and Np peaks with relevant parameters [7].

Element	Ion	Wavelength (nm)	Lower E (eV)	Upper E (eV)	Lower g	Upper g	TP (s^{-1})	Accuracy[a]
Sr	II	407.77	0	3.03968	2	4	1.41×10^8	AA
Sr	I	474.19	1.77514	4.38905	1	3	3.90×10^7	B+
Sr	I	552.18	2.25143	4.49618	3	3	6.30×10^7	A'
Sr	I	640.85	2.27130	4.20546	7	9	2.40×10^7	C+
Sr	I	650.40	2.25884	4.16459	5	7	2.00×10^7	C+
Sr	I	687.83	1.79831	3.60035	3	3	2.70×10^7	B+
Sr	I	707.01	1.84719	3.60035	5	3	4.20×10^7	B
Np	I	456.34	0.82369	3.53988	10	14	—	—
Np	II	538.10	0.67594	2.97941	9	9	—	—
Np	I	607.39	0	2.04070	12	10	—	—
Np	I	612.05	0	2.02516	12	14	—	—
Np	I	697.21	0	1.77780	12	12	—	—

[a]NIST TP accuracy definitions: AA ≤ 1%, A ≤ 3%, B+ ≤ 7%, B ≤ 10%, C+ ≤ 18% [7].

B. Saha–Boltzmann analysis

Peaks were fit with Voigt functions in Python using the lmfit library to calculate the integral intensity [17]. In addition to the Sr and Np peaks, the 656.28 nm H_α peak was fit to calculate the electron density (N_e) of the plasma according to the relationship in Eq. (1) where $FWHM_{H\alpha}$ is the full width half maximum of the H_α peak [18].

$$N_e = 10^{17} \times \left(\frac{FWHM_{H_\alpha}}{0.549}\right)^{1.4713} \quad (1)$$

The electron density for the first sample was calculated to be $2.88 \pm 0.310 \times 10^{17}$ cm^{-3}, which is a value on par with the expected levels for a laser induced plasma [18-20]. The next step to define the plasma was to calculate the plasma temperature. This can be performed by employing a Saha–Boltzmann plot, which relates the neutral and ionized peak areas to a combination of the transition parameters. The Saha–Boltzmann plotting relationship is defined as

$$y = \frac{-1}{T}x + ln\left(\frac{C_{s,1}}{U_{s,1}(T)}\right), \quad (2)$$

where

$$y = ln\left(\frac{I}{A_{nm}g_n}\right) + B \times \ln\left(\frac{2(2\pi m_e T)^{3/2}}{h^3 N_e}\right),$$
$$x = E_n + B \times E_{ion}, \quad (3)$$
$$and\ B = \begin{cases} 0\ for\ neutral \\ 1\ for\ ionized \end{cases}$$

where T is the plasma temperature (eV), $C_{s,1}$ is the number density of neutral species, $U_{s,1}(T)$ is the neutral species partition function at the plasma temperature, A_{nm} is the TP (s^{-1}), g_n is the upper-level degeneracy, m_e is the rest mass of an electron, h is Plank's constant, E_n is the upper energy level (eV), and E_{ion} is the ionization potential (eV) [11]. Since the y-coordinate for ionized species is dependent upon the plasma temperature, an iterative fitting procedure must be completed until the temperature from the slope of the fitted Saha–Boltzmann plot and the temperature input for the ionized species y-coordinate converges. A temperature of 0.600 eV was used to start the iterative fitting and the temperature quickly converged. The resultant temperature for the sample 1 was 0.570 ± 0.016 eV; again, this value agreed with reported laser induced plasmas [18-20]. The final Saha–Boltzmann plot for sample 1 is shown in Fig. 3.

To apply the Saha–Boltzmann methods, the plasma must be in a state of local thermodynamic equilibrium (LTE). As mentioned previously, typical CF-LIBS studies use nanosecond gating to truly measure the signal during the period of LTE. A laser induced plasma would not be in a state of LTE during its creation and expansion, nor later in its lifetime while rapidly cooling [2, 10]. The echelle spectrometer available for this study utilized an EMCCD which is unable to take measurements on this time scale. Previous studies have applied CF-LIBS procedures to spectra collected with similar exposure times with levels of success [18, 21-23]. Grifoni et al. investigated deriving the time resolved (TR) signal from the time integrated (TI) –

LIBS signal to compare their use in plasma analysis [10]. The study found the plasma temperature and electron density calculated from both TR and TI signals to be effectively equivalent. Colgan et al. also showed that the model calculated spectrum from an iron plasma in LTE and non-LTE at sufficiently high densities ($>10^{16}$ cm^{-3}) are quiet close [23]. Based on this, the assumptions of LTE were used in this study to investigate the effectiveness of the CF-LIBS methods given the experimental equipment available.

The McWhirter's criterion is often used to determine if the plasma could be in a state of LTE. The McWhirter's criterion compares the electron density to the plasma temperature and the largest energy transition as shown in Eq. (4), if it is true, then the assumption of LTE may be appropriate [19].

$$N_e(cm^{-3}) \geq 1.6 \times 10^{12} {T_e}^{1/2} (\Delta E)^3 \quad (4)$$

It is important to note that fulfillment of the McWhirter criterion is necessary, but not sufficient for assessing the validity of LTE in LIBS plasmas [24]. Based on the electron density and temperature calculated above, the McWhirter's criterion is satisfied. The current study assumes that the measured spectra reflect an effective LTE. By delaying the spectrometer, the beginning of the plasma lifetime when the system is not in LTE was not measured. The remaining of light emitted during the plasma lifetime was collected; however, given that plasmas cool exponentially an assumption that most of the collected signal was emitted during a state of LTE was made.

C. Transition probability calculation

With the Saha–Boltzmann line for Sr now established, the concepts typically used for CF-LIBS were used to determine the theoretical Saha–Boltzmann line for Np [18-20]. First, the number density of neutral Sr species was determined from the intercept of the Sr line (Eq. 2). The singly ionized number density was then calculated using the Saha equation:

$$\frac{C_{s,2}}{C_{s,1}} = \frac{6.04 \times 10^{21} T^{3/2} U_{s,2}}{N_e \quad U_{s,1}} e^{\left(-E_{ion}/T\right)}, \tag{5}$$

where 1 and 2 refer to the neutral and singly ionized species [11]. With this, the total number density (sum of neutral and ionized number densities) of Sr was calculated. Knowing the ratio of Np to Sr, the total number density of Np was calculated, and using the Saha equation, the ratio of neutral to singly ionized Np species was defined. The number densities of neutral and singly ionized Np species were then individually determined with these two relationships. The intercept of the Saha–Boltzmann line for Np was calculated next. The slope of both Saha–Boltzmann lines must be equal because the temperature of the plasma, regardless of species, is equal under the LTE assumptions. This provided a fully defined Saha–Boltzmann line for the Np in sample 1, which would be used to estimate the previously unreported TPs. The Saha–Boltzmann line for Np in sample 1 is shown parallel to the Sr line in Fig. 3.

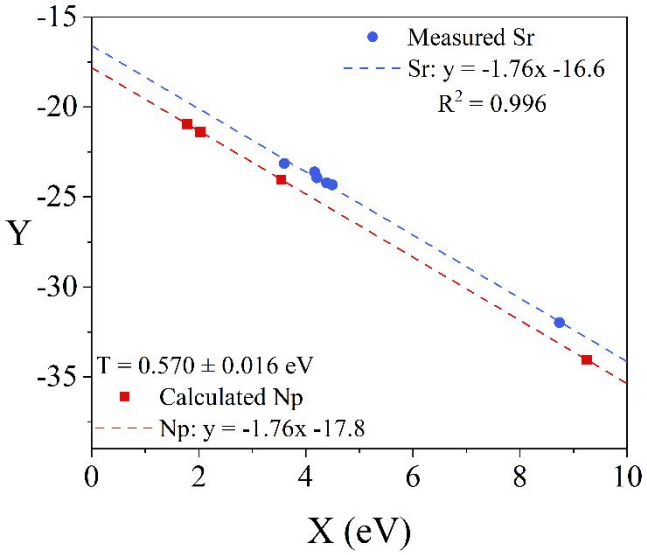

Fig. 3. The Saha–Boltzmann plot for sample 1 where the Sr line is shown in blue (upper line), and the Np line is shown in red (lower line). The Sr line was iteratively fit by adjusting the plasma temperature until convergence was achieved. The Np line is derived from the Sr trend based on the relations found in plasmas during an effective state of LTE.

For each Np peak, Eq. (2) was solved for the TP using the y-coordinates from the calculated Saha–Boltzmann line and the transition information detailed in Table I. The same procedure was applied to sample 2, and the electron density was calculated to be $3.29 \pm 0.395 \times 10^{17}$ cm^{-3}, the Sr Saha–Boltzmann line was defined, and the plasma temperature was calculated as 0.548 ± 0.016 eV. Again, the McWhirter's criterion was satisfied. The TPs calculated from sample 1 and 2 are shown in Table II. The values calculated from each sample agreed with one another and passed a two-tailed t-test for correlation at a confidence of 99%.

Table II. Calculated neutral and singly ionized Np TPs.

Element	Wavelength (nm)	TP (s^{-1}) Sample 1	Sample 2	Average
Np I	456.34	$1.25 \pm 0.357 \times 10^7$	$1.67 \pm 0.452 \times 10^7$	$1.46 \pm 0.461 \times 10^7$
Np II	538.10	$3.47 \pm 0.990 \times 10^7$	$9.49 \pm 0.305 \times 10^7$	$6.48 \pm 3.78 \times 10^7$
Np I	607.39	$9.08 \pm 2.57 \times 10^5$	$1.16 \pm 0.398 \times 10^6$	$1.04 \pm 0.359 \times 10^6$
Np I	612.05	$6.77 \pm 2.05 \times 10^5$	$8.60 \pm 3.90 \times 10^5$	$7.69 \pm 3.23 \times 10^5$
Np I	697.21	$9.23 \pm 2.70 \times 10^5$	$1.14 \pm 0.346 \times 10^6$	$1.03 \pm 0.323 \times 10^6$

D. Evaluating Np transition probabilities

The calculated Np TPs were validated by using those calculated from sample 1 to perform CF-LIBS on sample 2 to calculate the Np/Sr molar ratios and vice versa. Likewise, we can also use the averaged TPs for these calculations.

A Saha–Boltzmann line was built for each element, and the temperature is calculated through manual iterative fitting. The temperature fitting was completed two ways; first, the average slope of the two lines was iteratively fit and second, only the slope of Sr line was iteratively fit. The assumption of effective LTE that the temperature of the plasma is homogonous is used in the first case. The second case was also performed because Sr has more peaks, and the TPs have lower uncertainty (≤18%). Since the Np TPs were derived from those of Sr, they inherently have a greater uncertainty.

Once a convergent temperature was reached, the partition functions for neutral and singly ionized species of both elements were calculated. Using these values with the Saha–Boltzmann intercepts and the Saha equation (Eq. 5), the number density of the neutral and singly ionized species of both elements was calculated. The molar ratios were then calculated by dividing the total number density for each element. The resultant molar ratios for both samples calculated with these various TPs and temperature calculation methods are detailed in Table III. All molar ratios

calculated were within 10% of the known value; however, the average error is much lower at 3.86%.

Table III. Molar ratios of Np to Sr measured using CF-LIBS and calculated Np TPs.

Sample	Known Np/Sr Ratio	TP from opposite sample		Average TP	
		Using average T	Using Sr T	Using average T	Using Sr T
1	8.0	8.695	7.996	8.698	8.230
2	2.0	1.855	2.001	2.007	2.058

The third sample did not contain Sr, but the calculated TPs can still be used to determine the plasma temperature. The electron density was calculated from the H_α peak, the Saha–Boltzmann plot for Np was constructed (shown in Fig. 4), and the temperature was iteratively fit. The electron density was calculated to be $3.37 \pm 0.396 \times 10^{17}$ cm^{-3}, and the plasma temperature was calculated as 0.544 ± 0.003 eV. This sample also satisfied the McWhirter's criterion indicating the potential of LTE. Lastly, from the Saha–Boltzmann line and Saha equation, the total number density of Np was determined to be 2.64×10^{-6}. This value is greater than both the total number densities of Np calculated for samples 1 and 2, which were 1.40×10^{-6} and 8.96×10^{-7}, respectively. These values correlate with the increase in relative Np concentration and serve as another verification that CF-LIBS may be employed for analysis of Np in radiological hot cells or glove boxes.

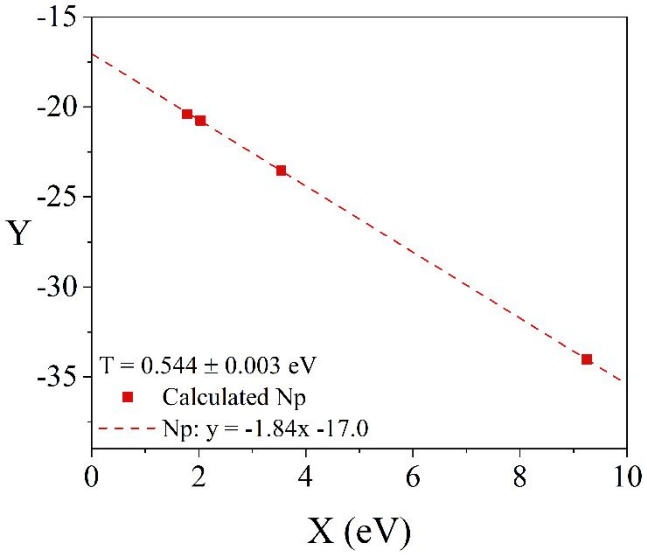

Fig. 4. The Saha–Boltzmann plot of sample 3 containing only Np calculated using newly determined TPs shows a strong linear fit ($R^2 = 0.999$).

IV. CONCLUSIONS

TPs are crucial pieces of fundamental knowledge necessary for CF-LIBS and other plasma analytical methods. Typically, the determination of these parameters requires sizable amounts of material and complex experimental systems [6]. By determining the first reported Np TPs, this study has reiterated that laser induced plasmas can be used to estimate TPs using only minor amounts of materials and using the same equipment required for later LIBS measurements. This opens the door to calculating the TPs of other actinide elements with little to no reported values. using the sample enclosure and analytical methods described here. Benefits of this technique include minimal sample preparation, small sample quantities, and the opportunity for remote analysis in restrictive glove box and hot cell environments.

The timeliness of the CF-LIBS analysis offers a large advantage compared to ICP-OES analysis (e.g., ~10 min vs ~60 min). Therefore, CF-LIBS may provide several operational and

scientific benefits for measuring actinide elements, many of which are rare, expensive, and highly radioactive. The methods shown in this study permit the future expanded use of CF-LIBS for applications within the nuclear fuel cycle and within medical isotope production.

The success of the calculated molar ratios also demonstrate that the assumption of effective LTE may be appropriate in some cases. Following the success of this study, future work should involve comparing results using time integrated EMCCD measurements and time resolved ICCD measurements, as well as how these different measurements impact the uncertainty of the calculated TPs.

ACKNOWLEDGMENTS

This work was supported by the ^{238}Pu Supply Program at the U.S. Department of Energy's Oak Ridge National Laboratory and by the U.S. Department of Energy Isotope Program, managed by the Office of Science for Isotope Research, Development, and Production.

FUNDING

Funding for this effort was provided by the Science Mission Directorate of NASA and administered by the U.S. Department of Energy, Office of Nuclear Energy, under contract DEAC05-00OR22725. This research is supported by the U.S. Department of Energy Isotope Program, managed by the Office of Science for Isotope R&D and Production.

REFERENCES

1. Andrews, H., J. McFarlane, D. Holcomb, D. B. Ezell, K. Myhre, A. Lines, S. Bryan, H. Felmy. Sensor technology for molten salt reactor off-gas systems. Proceedings of the 12th NPIC&HMIT. 723 (2021).

2. D. W. Hahn, N. Omenetto, Laser-induced breakdown spectroscopy (LIBS), Part I: Review of basic diagnostics and plasma–particle interactions: Still-challenging issues within the analytical plasma community, Appl. Spectrosc. **64**, 335A (2010).

3. D. W. Hahn, N. Omenetto, Laser-induced breakdown spectroscopy (LIBS), Part II: Review of instrumental and methodological approaches to material analysis and applications to different fields, Appl. Spectrosc. **66**, 347 (2012).

4. F. J. Fortes, J. J. Laserna, The development of fieldable laser-induced breakdown spectrometer: No limits on the horizon, Spectrochim. Acta - Part B At. Spectrosc. **65**, 975 (2010).

5. A. Ciucci, M. Corsi, V. Palleschi, S. Rastelli, A. Salvetti, E. Tognoni, New procedure for quantitative elemental analysis by laser-induced plasma spectroscopy, Appl. Spectrosc. **53**, 960 (1999).

6. G. Garcia, J. Campos, TPs for Triplet Levels of Sr(I), J. Quant. Spectrosc. Radiat. Transfer **39**, 477 (1988).

7. A. Kramida, Y. Ralchenko, J. Reader, NIST ASD Team, NIST Atomic Spectra Database (Ver. 5.7), National Institute of Standards and Technology. https://physics.nist.gov/asd.

8. W. L. Weise, G. A. Martin, Transition probabilities, Nat. Stand. Ref. Data Ser. NSRDS-68, 359 (1980).

9. L. R. Sadergaski, K. G. Myhre, L. H. Delmau, D. W. DePaoli, R. M. Wham, Status of spectroscopy and online monitoring for the Plutonium-238 Supply Program, ORNL/TM-2021/1922.

10. E. Grifoni, S. Legnaioli, M. Lezzerini, G. Lorenzetti, S. Pagnotta, and V. Palleschi, Extracting time-resolved information from time-integrated laser-induced breakdown spectra, J. Spectrosc. 849310 (2014).

11. F. d. O. Borges, J. U. Ospina, G. d. H. Cavalcanti, E. E. Farias, A. A. Rocha, P. I. L. B. Ferreira, G. C. Gomes, A. Mello, CF-LIBS analysis of frozen aqueous solution samples by using a standard internal reference and correcting the self-absorption effect, J. Anal. At. Spectrom. **33**, 629 (2018).

12. K.G. Myhre, M.J. Mehta, M.Z. Martin, M. Du. Laser Induced Breakdown Spectroscopy analysis of europium and samarium in aluminum oxide. Spectrochim. Acta - Part B At. Spectrosc. **149**, 30 (2018).

13. G. Van Rossum, F. L. Drake. *Python 3 Reference Manual*. Scotts Valley, CA. (2009).

14. P. Yaroshchyk, J. E. Eberhardt, Automatic correction of continuum background in laser-induced breakdown spectroscopy using a model-free algorithm. Spectrochim. Acta - Part B At. Spectrosc. **99**, 138 (2014).

15. E. L. DeKalb, M. C. Edelson, Atlas of atomic spectral lines of neptunium emitted by an inductively coupled plasma. AMES Laboratory Report IS-4933 (1987).

16. J. E. Barefield II, E. J. Judge, J. M. Berg, S. P. Willson, L. A. Le, L. N. Lopez, Analysis and spectral assignments of mixed actinide oxide samples using laser-induced breakdown spectroscopy (LIBS). App. Spectrosc. **67**, 433 (2013).

17. M. Newville, T. Stensitzki, D. B. Allen, A. Ingargiola, LMFIT: Non-linear least-square minimization and curve-fitting for Python. Zenodo (2014).

18. Z. Farooq, R. Ali, U. S. Qurashi, M. H.R. Mahmood, M. Yaseen, M. A. Qayyum, M. N. Hussain, S. M. Shah, T. Jan, Spectroscopic studies of laser produced plasma of doped nano-structured material by laser induced breakdown spectroscopy, Physics of Plasmas, **25**, 093106 (2018).

19. S. Yalcin, D.R. Crosley, G.P. Smith, G.W. Faris, Influence of ambient conditions on the laser air spark, App. Phys. B **68**, 121 (1999).

20. E. Mal, R. Junjuri, M. K. Gundawar, A. Khare, Optimization of temporal window for application of calibration free-laser induced breakdown spectroscopy (CF-LIBS) on copper alloys in air employing a single line, J. Anal. At. Spectrom. **34**, 319 (2019).

21. Z. A.Umar, U. Liaqat, R. Ahmed, R. Hedwig, M. Ramli, M. A. Marpaung, K. H. Kurniawan, M. Pardede, M. A. Baig, Determination of Micronutrients and Toxic Elements in Moringa Oleifera Leaves by Calibration Free Laser-Induced Breakdown Spectroscopy (LIBS), Anal. Lett. (2021).

22. L. Sheng, T. Zhang, K. Wang, H. Tang, H. Li, Quantitative analysis of Fe content in iron ore via external calibration in conjunction with internal standardization method coupled with LIBS, Chem. Res. Chin. Univ. **31**: 107–111 (2015).

23. J. Colgan, E.J. Judge, D.P. Kilcrease, J.E. Barefield, Ab-initio modeling of an iron laser-induced plasma: Comparison between theoretical and experimental atomic emission spectra, Spectrochim. Acta - Part B At. Spectrosc. 97: 65-73. (2014).

24. G. Cristoforetti, A. De Giacomo, M. Dell'Aglio, S. Legnaioli, E. Tognoni, V. Palleschi, N. Omenetto, Local Thermodynamic Equilibrium in Laser-Induced Breakdown Spectroscopy: Beyond the McWhirter criterion, Spectrochim. Acta - Part B At. Spectrosc. **65**(1): 86-95. (2010).